Environmental Science Nano

ROYAL SOCIETY OF CHEMISTRY

PAPER

View Article Online
View Journal | View Issue

Cite this: *Environ. Sci.: Nano*, 2025, 12, 2395

Poly(lactic acid) nanoplastics through laser ablation: establishing a reference model for mimicking biobased nanoplastics in aquatic environments†

Malavika Manju Sudheer,[ab] Arezou Fazli,[a] Stefania Sganga,[c] Nicola Tirelli,[c] Riccardo Carzino,[d] Marina Veronesi,[e] Kirill Khabarov,[f] Athanassia Athanassiou[a] and Despina Fragouli*[a]

Received 24th September 2024,
Accepted 24th February 2025

DOI: 10.1039/d4en00891j

rsc.li/es-nano

Due to the well-documented negative environmental impacts of conventional plastics, the use of bioplastics has been increasing. Poly(lactic acid) (PLA) is currently among the most common and industrially available bioplastics. Although PLA is compostable under industrial conditions and generally degrades more quickly than conventional plastics, its breakdown in typical environmental settings remains problematic. PLA's potential to contribute to plastic pollution, by releasing microplastics and nanoplastics, makes it crucial to understand how these particles behave, especially in marine environments. However, as for all nanoplastics, identifying, isolating, and quantifying PLA nanoplastics in water presents significant challenges. This study proposes a versatile approach to fabricate PLA nanoplastics through laser ablation in a water environment to mimic real-world samples. Commencing with bulk PLA films, this top-down method yields the formation of nanoplastics with an average diameter of 54.7 ± 26.7 nm. Surface and chemical analyses confirm the presence of carboxylic groups on their surface, potentially resembling the environmental degradation pathway of PLA under exposure to sunlight and humid environments. This indicates that the proposed process results in a PLA nanoplastics system that serves as an invaluable reference model, enabling realistic environmental scenario explorations and simulations for risk assessment evaluations on bio-based nanoplastics.

Environmental significance

The well-established environmental impact of petroleum-based polymers has driven the development of biobased polymers as valuable alternatives. One of the most popular biopolymers is poly(lactic acid) (PLA), which is completely biodegradable under strictly controlled conditions. This suggests that, if not properly managed, PLA could potentially undergo environmental aging, leading to the formation of nanoplastics similar to its synthetic counterparts. This raises the need to expand our knowledge on the fate of PLA-based debris, with a particular focus on the environmental and biological fate of PLA nanoplastics. Currently, due to the inherent challenges in isolating and identifying real-field samples, most studies on nanoplastics are based on chemically synthesized conventional plastics. These particles, however, do not adequately represent environmentally relevant reference models of bioplastic origin. In this context, we propose a single-step fabrication method using laser ablation to create PLA nanoplastics that could serve as a reference model for realistic environmental scenarios. This approach provides a reliable tool for investigating the fate and effects of the bio-based plastic litter in different environments.

[a] *Smart Materials, Istituto Italiano di Tecnologia, via Morego 30, 16163 Genova, Italy. E-mail: despina.fragouli@iit.it*
[b] *Dipartimento di Chimica e Chimica Industriale, Università degli Studi di Genova, via Dodecaneso 31, 16146 Genova, Italy*
[c] *Laboratory of Polymers and Biomaterials, Istituto Italiano di Tecnologia, via Morego 30, 16163 Genova, Italy*
[d] *Materials Characterization Facility, Istituto Italiano di Tecnologia, via Morego 30, 16163 Genova, Italy*
[e] *Structural Biophysics Facility, Istituto Italiano di Tecnologia, via Morego 30, 16163 Genova, Italy*
[f] *Plasmon Nanotechnologies, Istituto Italiano di Tecnologia, via Morego 30, 16163 Genova, Italy*

† Electronic supplementary information (ESI) available. See DOI: https://doi.org/10.1039/d4en00891j

Introduction

Since the advent of the first synthetic polymer, plastics have proliferated exponentially, driven by mass production and rapid expansion. Among the most prevalent are thermoplastic polymers, like polyethylene terephthalate (PET), polyethylene (PE), polyvinyl chloride (PVC), polypropylene (PP), polycarbonate (PC), and polystyrene (PS), all derived from non-renewable petrochemical sources.[1] These polymers, engineered to be low-cost and highly adaptable, exhibit resilience against various environmental factors such as microbial degradation, light exposure, and

water permeation. This durability makes them indispensable for everyday applications, such as packaging and biomedical. However, their longevity poses a significant environmental threat when they are exposed to the environment in the form of plastic litter.[2–4]

In fact, according to the Global Plastics Outlook report published in 2022 by the Organization for Economic Co-operation and Development (OECD), only 9% of the produced plastic waste undergoes recycling, while 19% is incinerated.[5] The remaining amount is either deposited in landfills (50%) or not managed with any of the processes mentioned above (22%), ultimately finding its way into aquatic ecosystems, where it accumulates over time.[6] Specifically, long-term projections suggest an alarming escalation in mismanaged plastic waste, reaching over 270 million metric tons by 2060.[5] Such projections underscore the urgent need to address the pervasive issue of plastic waste accumulation and the resulting profound ecological ramifications.

These concerns surrounding the widespread use of petroleum-based plastics and their enduring presence in the environment have prompted efforts to explore alternative and more environmentally friendly materials, such as bio-based and biodegradable plastics. One such alternative gaining traction is poly(lactic acid) (PLA), a thermoplastic polymer lauded for its bio-based origin and biodegradability under controlled conditions. PLA presents a promising solution to mitigate the environmental impact of petroleum-based plastics, offering similar versatility, processability, and functionality as conventional counterparts for specific applications.[7] In fact, due to all these properties, PLA has earned the title of the "polymer of the 21st century".[8,9] However, studies reveal that the biodegradability of PLA is limited to specific composting conditions, requiring an oxygen-rich environment under controlled temperatures (58–80 °C) and humidity (>60%).[10] This raises concerns about its eventual persistence in natural environments, resembling its petroleum-based counterparts, particularly in marine settings where temperatures are lower.[2] PLA waste in the environment may undergo various degradation pathways such as photo and thermal-oxidation, hydrolysis, mechanical fragmentation, *etc.*[2,11,12] to form microplastics (MPs) and nanoplastics (NPs). NPs are plastic fragments of size <1000 nm,[13] with altered chemical and structural properties compared to their bulk, and are considered contaminants of emerging concern.[13,14] As utilization of PLA increases, it is important to expand our knowledge of the formation pathways of PLA NPs, their presence in the environment, and their environmental fate.

Multiple recent studies have been conducted to explore the possible release of PLA MPs and NPs from commercial products such as PLA-lined paper cups[15] and tea bags,[16] as well as the formation of secondary fragments under UV photoaging, mechanical, biological, and enzymatic degradation of PLA macroplastic components.[17–19] Despite confirming the release of PLA NPs under environmental stressors in well-controlled experimental conditions, studies on the presence of PLA NPs in environmental samples present a multifaceted research challenge. This stems from the diversity of the properties of plastic sources, usage patterns, and different waste management strategies linked to the disposal of plastics. Consequently, there are numerous emission pathways for MPs and NPs. Therefore, the properties of the generated particles may also reflect these diversities,[20–23] which, in combination with the various interactions that NPs may have with various environmental components, result in NPs with a wide range of physical and chemical properties in the actual field samples. On top of that, studies have shown that the environmental concentrations of NPs are extremely low, ranging between 0.04–1.17 μg L^{-1} (depending on the NPs and water type).[24] Considering also the fact that the environmental samples usually contain a great variety of organic matter makes the NPs identification and quantification akin to searching for a needle in a haystack.[25]

Recently, studies have begun to shed light on the effects of PLA MPs and NPs on organisms, using either commercially available particles[26,27] or PLA NPs prepared through bottom-up chemical methods such as solvent evaporation combined with mini-emulsion techniques.[28,29] Nevertheless, these studies may not fully capture the characteristics of environmentally relevant NPs, which often exhibit irregular shapes and complex surface chemistry. Despite the extensive endeavors to create representative reference NPs models using top-down techniques like milling processes[30,31] and laser ablation,[32,33] based on current knowledge, these are mainly focused on conventional plastics. In fact, there seems to be a gap in such efforts regarding commonly used bio-based PLA, underscoring the need to expand investigations toward the development of more representative reference models for studying the fate of PLA NPs. Understanding their distinctive properties and environmental behavior holds profound benefits for ecosystems, health, and human well-being in the foreseeable future.

With this study, we explore the present versatility of laser ablation, a reagent-free approach for NPs fabrication,[32,34] to develop PLA NPs that closely mimic their expected properties in natural environmental conditions. The aim is not only to produce a bio-based NPs reference model but also to explore in-depth the actual modifications induced to the polymer during the NPs fabrication and to correlate them with the natural degradation pathways of PLA debris. Through the irradiation of a bulk PLA film immersed in water using an excimer pulsed laser with an excitation wavelength of 248 nm, PLA NPs with an average diameter of 54.7 ± 26.7 nm were successfully synthesized directly in the water medium. Chemical characterization of the resulting NPs reveals potential surface modifications consistent with the environmental degradation pathways of PLA. The as-fabricated PLA NPs serve as invaluable reference models for studying the environmental fate of such particles, enabling more realistic environmental assessments. Therefore, the presented outcomes contribute to advancing our understanding of PLA NPs and underscore the importance of considering bio-based polymeric fragments in environmental research.

Materials and methods

Materials

Extruder grade PLA pellets (grade: 2003D, cas-no.: 9051-89-2) were supplied by NatureWorks. UranyLess EM (electron microscopy grade) contrast stain solution used for transmission electron microscopy (TEM) studies was purchased from Delta Microscopies. Tris(hydroxymethyl) aminomethane hydrochloride salt (Trizma hydrochloride, cas-no.: 1185-53-1, pH 7.0–9.0, 0.002 M, purity ≥99%), phosphate buffered saline (cas-no.: P3813, pH 7.4, 0.002 M), acetic acid (cas-no.: 64-19-7, purity ≥99.8%), sodium hydroxide (cas-no.: 1310-73-2, purity ≥98%), isopropanol (cas-no.: 67-63-0, purity ≥99.5%), as well as chloroform ($CDCl_3$, cas-no.: 865-49-6, 99.9 atom% D) and deuterium oxide (D_2O, cas-no.: 7789-20-0, 99.9 atom% D) used for NMR analyses, were all purchased from Sigma-Aldrich.

Fabrication of PLA films

To prevent interaction with air and moisture, the PLA pellets were initially dried in a vacuum oven at 60 °C for 24 hours. Subsequently, the pellets were processed using an IKA Pilotina MC dry miller equipped with a sieve with a pore size of 3 mm. The resultant PLA powder, with a particle size of ≤3 mm, underwent an additional vacuum drying step under identical conditions, as previously referred, to ensure optimal dryness before film preparation. PLA films were then fabricated following a compression molding process using a Carver 4122 hot press. Precisely, 12 mg of the ground PLA powder was placed between two metal frames lined with Teflon sheets to prevent adhesion during the pressing process. This assembly was subsequently introduced between hot plates preheated to 180 °C. Initially, the polymer was allowed to melt for 5 minutes without any applied pressure. Following this, a pressure of 4 metric tons was applied for 10 minutes to ensure proper molding and cohesion of the PLA. Once the pressing cycle was completed, the plates were left to naturally cool down to room temperature, forming the desired flat PLA films with a thickness of 1 mm and an area of 100 cm^2.

Fabrication of PLA NPs by laser ablation

Before laser treatment, the produced PLA films were meticulously cleaned using isopropanol, followed by Milli-Q water washing steps. The laser ablation was performed by exposing a 6 cm^2 segment of the PLA film immersed in 8 mL of Milli-Q water to pulsed UV laser irradiation (ESI† Fig. S1) using a KrF excimer laser (irradiation wavelength 248 nm, pulse duration of 20 ns, repetition rate of 10 Hz, Coherent-CompexPro 110) coupled with a micromachining apparatus (Optec-MicroMaster). The laser ablation was performed by 50 pulses, at a fluence of 3.5 J cm^{-2}, to produce an ablation spot of 450 × 450 μm. One complete ablation cycle consists of 144 ablation spots, arranged in a 12 × 12 grid format (ESI† Fig. S2). To obtain an ablation product with a high number of NPs, 32 ablation cycles were executed, and the resultant dispersion was concentrated using a rotavapor set at 45 °C. For the chemical characterizations of the NPs, the concentrated samples underwent centrifugation (utilizing a Sartorius, Centrisart G-16C centrifuge) at 21 000 × *g* for a duration of 10 minutes at 23 °C. After the removal of the supernatant, the precipitated material was resuspended in approximately 20 μL of Milli-Q water and subsequently used for further characterization.

NPs characterization

The morphology of the NPs was examined using transmission electron microscopy (TEM) (Jeol JEM 1400 Plus) imaging. Before the analysis, the concentrated samples were sonicated for 1 minute to ensure the uniform dispersion of particles. After sonication, samples were stained with UranyLess EM contrast stain solution for 30 seconds and were deposited onto a copper (Cu) grid pre-coated with an ultra-thin layer of amorphous carbon film, ensuring optimal contrast and visualization during TEM analysis. Multiple images were captured and analyzed using the ImageJ and OriginPro 2020 software to obtain the size distribution of the observed NPs.

The hydrodynamic size distribution and the concentration of the formed NPs were quantified using nanoparticle tracking analysis (NTA) with the Malvern NanoSight Pro 300 (Malvern Panalytical), equipped with the NTA software version 3.4. Samples from different ablation cycles were analyzed to compare the repeatability of the process. For this analysis, a volume of 1 mL from the vortexed sample was introduced into the NTA system *via* a syringe pump, operating at a rate of 50 AU. The particles were detected by blue laser (λ = 488 nm) camera-type sCMOS, providing the requisite sensitivity and resolution for accurate particle tracking and quantification.

Zetasizer Nano ZS (Malvern Instruments) was used to assess the surface charge characteristics of the produced NPs across varying pH values. To obtain the necessary pH values, aliquots of 300 μL of the ablation product were mixed with 700 μL of the different buffers prepared from tris(hydroxymethyl)aminomethane hydrochloride salt (Trizma hydrochloride) in Milli-Q water (pH 9–8, 0.002 M), phosphate buffer saline in Milli-Q water (pH 7–6, 0.002 M), and diluted acetic acid (0.002 M) in Milli-Q water with sodium hydroxide (pH 5–3, 0.002 M).

The NPs, concentrated through rotavapor and centrifugation, were resuspended in Milli-Q water and carefully drop-casted onto pre-cleaned and dried silicon wafer for Raman spectroscopy analysis (ESI† Fig. S3). For a comparative analysis, a pristine PLA film, cleaned with isopropanol and Milli-Q, was also examined. The Raman spectra were acquired utilizing the Renishaw inVia confocal Raman microscope, equipped with a CW DPSS laser with a wavelength of 532 nm. The spectral data were captured over the 600–3100 cm^{-1} range under the confocal settings using

the 150× objective, with an accumulation time of 120 seconds at a laser power density of 50 kW cm^{-2}. After data acquisition, data analysis and processing were executed using the built-in Wire 5.5 software platform.

The surface composition of NPs was elucidated through X-ray photoelectron spectroscopy (XPS) using a Kratos Axis UltraDLD instrument. The concentrated NPs were drop-casted on a precleaned and dried indium (In) substrate. A comparative analysis was also performed on the PLA film, which was cleaned with isopropanol and followed with Milli-Q water. A monochromatic Al Kα source acquired both survey and high-resolution spectra, operating at 20 mA and 15 kV. The survey spectra were obtained with a pass energy set at 160 eV, an energy step of 1 eV, and an analyzed area spanning 300 × 700 μm^2. Concurrently, high-resolution spectra were recorded within the same designated area, utilizing a pass energy of 20 eV and an incremental energy step of 0.1 eV. The Kratos charge neutralizer system was consistently applied across all samples to ensure accurate data interpretation. Furthermore, for precise binding energy scale calibration, the position of the dominant C 1s peak was standardized at 285 eV, representative of C–C bond configurations. Subsequent data analysis and interpretation were conducted utilizing the Casa XPS software.

The NMR analysis was also performed on the ablation product to identify the molecular components and to confirm the chemical nature of the formed NPs. To allow the characterization of the solid fraction, considering that polymer chains form this, the concentrated NPs (prepared following the same protocol explained previously) were resuspended in $CDCl_3$ and D_2O in a 1 : 1 ratio. The obtained dispersion was subsequently centrifuged for 30 minutes at 3200 rpm to separate the D_2O part from the $CDCl_3$ and to allow the two phases collection. The $CDCl_3$ can dissolve PLA and is expected to contain all the molecular polymeric components in its volume. In contrast, the D_2O phase may contain the polar molecular components of the ablation product distributed in the water medium during the ablation process. For the comparative studies, 5 mg of pristine PLA was dissolved in 500 μL of $CDCl_3$ and was vortexed for 30 minutes. The ^1H NMR spectra were recorded using Bruker FT NMR Neo 600 MHz spectrometer, equipped with a 5 mm Cryoprobe™ QCI $^1H/^{19}F$ $^{13}C/^{15}N$-D and an automatic sample changer, SampleJet™, with temperature control. The spectra were collected with the Bruker zg30 sequence, with a 30-degree flip angle, TD 64 K, a spectral width of 30 ppm, an acquisition time of 1.835 seconds, a number of 2048 scans, and a relaxation delay of 4 seconds.

Results and discussion

As shown in Fig. 1(a), the TEM analysis of the concentrated ablation product reveals the presence of particles with irregular shapes and broad size distribution. In particular, there are particles that present enhanced roundness, while others are elongated or of a more irregular shape. The particle size distribution presented in Fig. 1(b) shows that particles have a nanoscale size ranging between 10–125 nm, with an average diameter of 54.7 ± 26.7 nm. TEM images were captured from different spots across the sample (ESI† Fig. S4) to ensure an objective size analysis.

To further explore the size distribution and quantify the number of particles in the ablation product, the NTA analysis was employed. As depicted in Fig. 2, in agreement with the TEM study, the produced nanoparticles have heterogeneous size distribution, with most of them presenting hydrodynamic sizes ranging between 50–200 nm, with a mean size of around 127.4 ± 42.9 nm in the aqueous medium. A substantial proportion, encompassing about 90% of the particles, has diameters not exceeding 185 nm. In contrast, a minor fraction, constituting 10% of the particles detected, exhibited a hydrodynamic diameter of less than 75 nm. To explore if the adopted method results in a reproducible fabrication process, the NTA analysis was performed on samples from different ablation cycles. As shown in Table S1 and Fig. S5 of the ESI,† the concentration and size distributions were comparable across NPs produced from different ablation cycles, confirming the reproducibility of the fabrication process. From such analyses, we may conclude that each ablation cycle yields 2.35 × 10^9 ± 2.15 × 10^9 particles per mL.

The TEM and NTA analyses confirm the formation of nanoparticles as the result of interaction between the high-

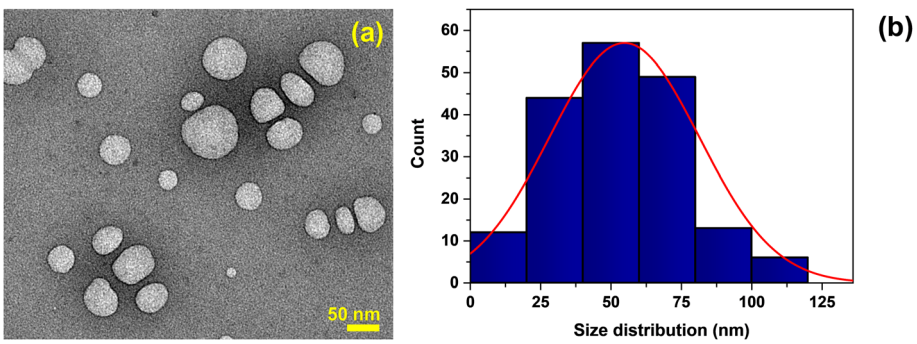

Fig. 1 (a) TEM micrograph of the formed nanoparticles. (b) The size distribution of nanoparticles was calculated from TEM micrographs using ImageJ software on a total of 180 particles.

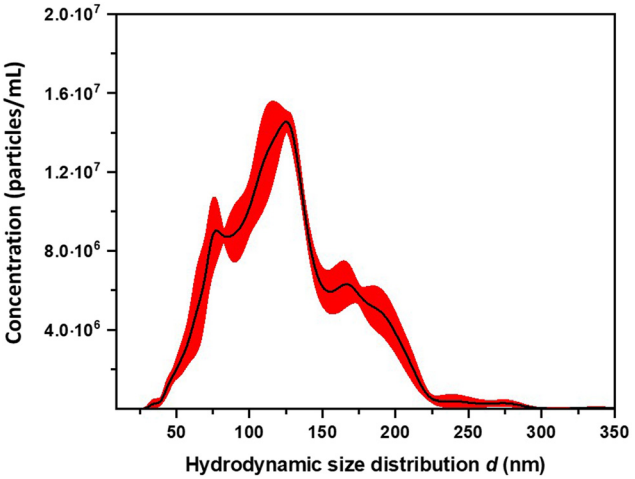

Fig. 2 The total concentration of the nanoparticles produced in the aqueous dispersion and their hydrodynamic size distribution derived from NTA analysis as observed from five consecutive measurements on the same sample, with the black line representing the mean hydrodynamic diameter and the red showing the standard deviation.

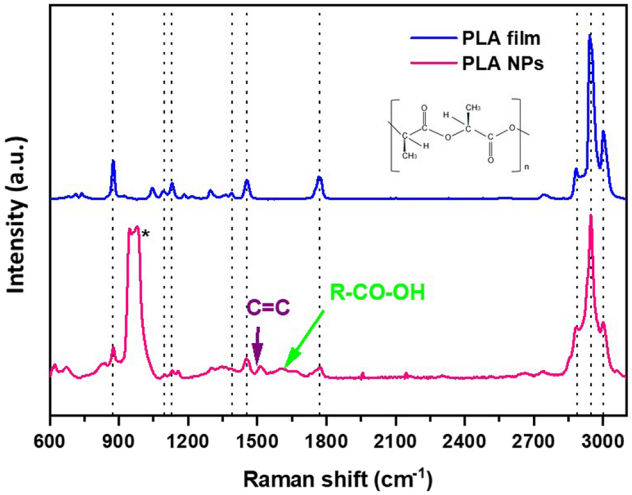

Fig. 3 The comparative Raman spectra of pristine film and of PLA NPs. The * corresponds to the Si peak, the substrate on which samples were deposited for the analysis.

energy UV pulsed laser beam and the polymeric surface. The formation of these particles, starting from the polymer film immersed in water, may be attributed to one of the two main ablation pathways: condensation or fragmentation. Condensation is a purely thermal pathway that follows the atomization of polymeric matter upon photon absorption. The carbon vapor formed during the heating phase condenses upon saturation in the plume, primarily forming carbon-based nanoparticles.[35] On the other hand, fragmentation is a mechanical effect attributed to the hydrodynamical expansion of the heated volume of the polymer target. It breaks the polymeric material into small particles due to the rapid thermoelastic expansion and tensile. Therefore, it may be a low-temperature pathway preserving the chemical structure of the polymer, mainly resulting in the formation of polymer-like nanoparticles.[35] It is essential to note that the presented approach, as well as the properties of the resulting particles, are intricately linked to the inherent characteristics of the polymer, such as its thermal conductivity, polymerization process, absorption properties, and the specific operational parameters of the laser system employed.[34,36,37] It should also be emphasized that there is no ionization and decomposition of water, as it is less likely to happen in a nanosecond laser processing underwater.[38]

To evaluate the chemical nature of the formed particles, Raman analysis was performed on the ablation product, and the obtained spectrum was compared with that of the pristine PLA film. As shown in Fig. 3, the Raman spectrum of pristine PLA depicts all the characteristic peaks of the PLA,[39] with the prominent peaks at 873 and 1768 cm^{-1} to indicate the out-of-phase C–O–C and carbonyl stretching of the polymer chain, respectively. The two peaks at 1044 and 1129 cm^{-1} denote the C–CH_3 bond stretch,[39] while the vibrational signatures associated with the symmetric and asymmetric deformation modes of CH_3 groups are visible at 1392 cm^{-1} and 1455 cm^{-1}, respectively. Furthermore, the symmetric and asymmetric stretching modes of CH_3 groups were observed at 2944 cm^{-1} and 3002 cm^{-1}, respectively.[40] Finally, the symmetric stretching mode of the C–H bonds is evident at 2866 cm^{-1}. A comprehensive analysis of the ablation product spectrum underscores that the generated particles retain all the distinctive peaks representative of the PLA polymer, proving that the formed particles have the PLA polymeric nature, suggesting the formation of NPs through the fragmentation ablation pathway. Interestingly, additional peaks also appear, postulated to arise from the degradation effects induced by the laser ablation of the film in water, targeting the ester bonds within the PLA matrix, confirming the formation of different chemical groups not initially part of the PLA polymer.[41] Specifically, a closer look at the Raman spectrum shows additional peaks between the 1620–1680 cm^{-1} range, which can be attributed to C=C and the out-of-the-phase stretching of carboxylic groups.[42] The appearance of the double-bonded carbon peak indicates the presence of alkanes or cyclic compounds.[43]

The presented results so far effectively confirm the formation of PLA NPs upon laser ablation of PLA films. Their shape and broad size distribution are in agreement with recent studies on environmentally relevant secondary PLA NPs.[44] Nonetheless, NPs originating from different environmental degradation pathways are proven to comprise diverse surface chemistry.[14,45] To explore the surface characteristics of the formed PLA NPs, their colloidal stability, and to verify any resemblance with those anticipated during the aging of environmentally exposed samples, the surface charge and the XPS analyses of the NPs were performed. The zeta potential of the as-generated PLA NPs was −37.6 ± 4.6 mV in the water dispersion after the laser ablation process, with pH ranging between 6.5–7, indicating a good colloidal stability, in agreement with what was observed by Banaei *et al.*[16] for PLA

NPs (~280 nm) released from commercial tea bags, and by Zhang *et al.*[46] on photo-aged PLA NPs. Through the pH modification of the NPs medium, it can be observed that the zeta potential increases in absolute values as the pH increases. These changes are more evident in the 5–8 pH range. This behavior is characteristic of the presence of weak acidic groups on the NPs surface, possibly arising from the surface oxidation of the PLA and cleavage of polymeric chains induced upon exposure to UV-pulsed laser irradiation during ablation.[47] Such processes can form weak acidic groups on the NPs surface, imparting a negative surface charge at the NP–water interface.[48] As shown in Fig. 4, by increasing the pH of the solution, the deprotonation of the weak acidic groups leads to the formation of a more negative surface charge. On the contrary, these groups undergo protonation under acidic conditions, shifting the surface charge towards more positive values.

The surface chemistry of the produced PLA NPs was also explored by XPS. As shown in Fig. 5(a), the deconvolution of the C1s of the pristine PLA film indicates the contribution of three characteristic peaks at 285.0, 287.0, and 289.0 eV attributed to the C–C or to the C–H bonds, to the C–O–C═O, and to the O═C–O bonds respectively[49] (also refer ESI† Table S2). In the case of the PLA NPs, as in Fig. 5(c), in addition to the characteristic peaks of PLA, two additional peaks at 285.7 and 287.2 eV appear, corresponding to the hydroxyl (–COH) and carbonyl (C═O) polar functional groups, confirming the observations of the zeta potential analysis. Analogous changes were observed in PLA films treated with ns (248 nm) and fs (515 nm) laser pulses,[50,51] with UV lamps,[52] and environmental factors (light, humidity, and temperature),[53] indicating that these changes can be attributed to the aging of PLA under the influence of laser irradiation in the presence of water.

On the other hand, the O1s spectra of pristine PLA film and PLA NPs presented in Fig. 5(b) and (d) possess two characteristic peaks at 532.2 and 533.2 eV corresponding to the ester (O═C–O–C) and ether (C–O–C) in the main polymer chain.[49] In the deconvolution of the O1s, the atomic percentages (refer to ESI† Table S3) of C–O decrease while C═O increases in the PLA NPs compared to the pristine PLA. These changes and the presence of additional surface groups indicate the modifications in PLA due to the adopted laser ablation process.

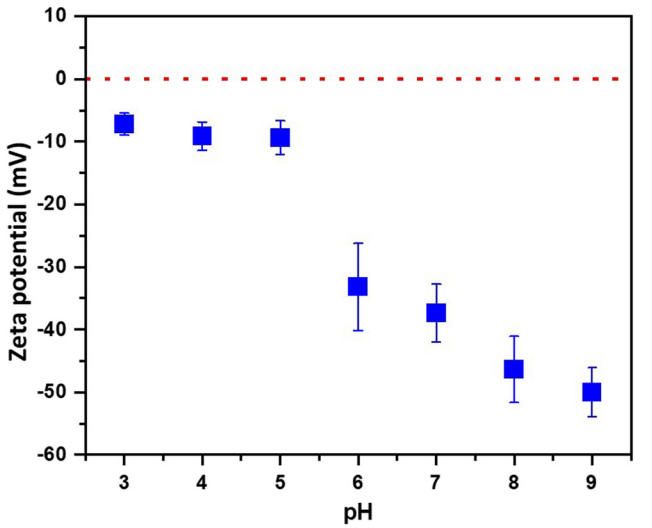

Fig. 4 Zeta potential of the NPs in aqueous environments of different pH values.

To further investigate the chemical nature of the formed particles in the water and identify any degradation by-products, NMR analysis was also performed. According to Fig. S7 in the ESI,† the NMR spectrum of the pristine PLA film dissolved in $CDCl_3$ is in accordance with what was reported in the literature.[54,55] Some additional signals observed can be attributed to the different forms of the PLA, such as poly(L-PLA), poly(*rac*-PLA), isotactic PLA, or syndiotactic PLA.[48,54] Similarly, as shown in Fig. 6(a), the NMR spectrum of the ablation product in $CDCl_3$ resembles the spectrum of the pristine PLA film, confirming, as in the case of the Raman study, that the formed NPs are of PLA nature.[55] Additional peaks attributed to the D_2O residue and the $CDCl_3$ solvent are also present in the spectrum of PLA NPs. Furthermore, a peak attributed to formic acid is also evident, in agreement with Therias *et al.*, who also detected formic acid in minor proportions after the photo-oxidation of PLA along with other low molecular weight photoproducts,[56] as well as with what was observed by Magrì *et al.*[32] in PET NPs fabricated by laser ablation. In the aliphatic region of the spectrum (Fig. 6(b)), other than the expected signals corresponding to PLA, many additional signals appear, which could be attributed to the possible presence of different chain lengths and forms of PLA. Interestingly, as depicted in Fig. 6(c), some unexpected signals related to the aromatic molecules were observed (also refer ESI† Fig. S8), which could be attributed to the production of aromatic molecules due to the possible thermal degradation of PLA,[44] as reported previously. In particular, Lomakin *et al.*, evaluating the photodegradation of PLA under UV radiation, observed weak signals corresponding to the double bond of the C═C–C(O)O– group,[57] absent in the pristine PLA. However, in the present case, the concentration of these substances is too low to allow their identification through 2D NMR and/or ^{13}C NMR analyses. To sum up, the NMR analysis of the ablation product confirms that the NPs formed by laser ablation are indeed PLA-based. The main structural fragments of PLA are preserved, while polymeric units of varying chain lengths and molecular structures also appear, likely due to the degradation process during their formation.

The NMR analysis of the D_2O fraction (Fig. S9†) showed the presence of lactic acid; the different NMR signals could be due to the presence of various forms of lactic acid, like monomer, dimer, and trimer. Also, we observed different solvent residual impurities in this spectrum, like ethanol, methanol, acetone, and acetic acid, at different concentrations, probably due to the sample handling using

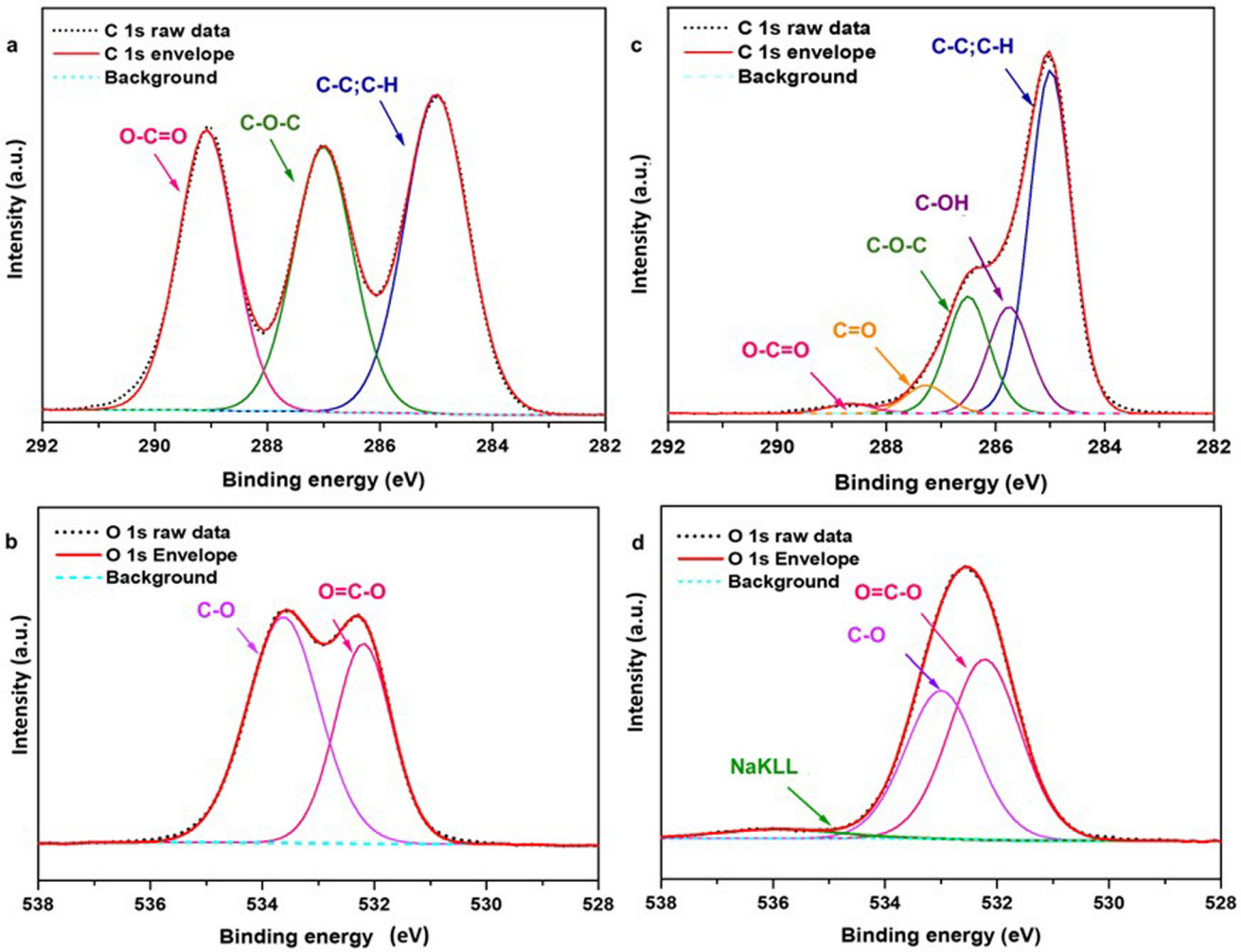

Fig. 5 XPS spectra; (a and b) C 1s and O 1s spectra of PLA film. (c and d) C 1s and O 1s spectra of PLA NPs. Additional oxygen bonds are attributed to the substrate (InOx) and possible impurities during the sample preparation process (see also ESI† Fig. S6).

rotavapor. Only the NMR signals of formic acid and $CDCl_3$ are visible in the aromatic region.

The so-far performed analysis of the formed NPs reveals their PLA chemical nature and a significant surface chemistry modification. The low concentration of the potential by-products hindered the ability to conduct supporting analyses necessary for defining a specific degradation mechanism during the adopted fabrication process. It should be noted that further studies fully elucidate the by-products to gain a comprehensive understanding of the extent and precise mechanisms underlying these degradation pathways of PLA NPs formed through laser ablation.

However, it is essential to note that the typical environmental degradation pathways of PLA have been well-established in the literature.[2,10,43] Excluding biodegradation, according to Fig. 7, the degradation of PLA involves hydrolysis (pathway A), photo-oxidation (pathway B), thermo-oxidation (pathway C), or a combination of these processes.[2]

According to pathway (A), the hydrolytic degradation of PLA under the influence of water and heat occurs *via* chain cleavage of ester groups, preferentially in the amorphous regions,[58] leading to an increase in the concentration of carboxylic acid end chains. These carboxylic end groups and their oligomers can catalyze the breakage of ester linkage during hydrolysis, forming acid groups. In the present study, the detection of additional polar groups on the surface of the NPs, along with their negative charge, could be indicative of the formation of carboxylic end-group compounds due to the hydrolytic degradation of the PLA during ablation.

In addition, considering pathway (B), the photo-oxidative degradation of PLA happens *via* the dissociation of C–O and C═O bonds in the presence of UV radiation below 280 nm.[59] The photodegradation of PLA mainly follows the Norrish type II mechanism, in which an excited state carbonyl abstracts an α-H to yield carboxylic acid and vinyl chain ends groups. The main chain scission in PLA can also lead to the formation of C═C bonds, where the electron transition at C═O triggers the reaction.[60] Lomakin *et al.*[57] have also reported a similar formation of C═C bonds with the participation of CH_3 groups associated with the photodissociation of PLA following the Norrish II mechanism. However, the weak signals corresponding to these peaks in the analyses could indicate the weakly

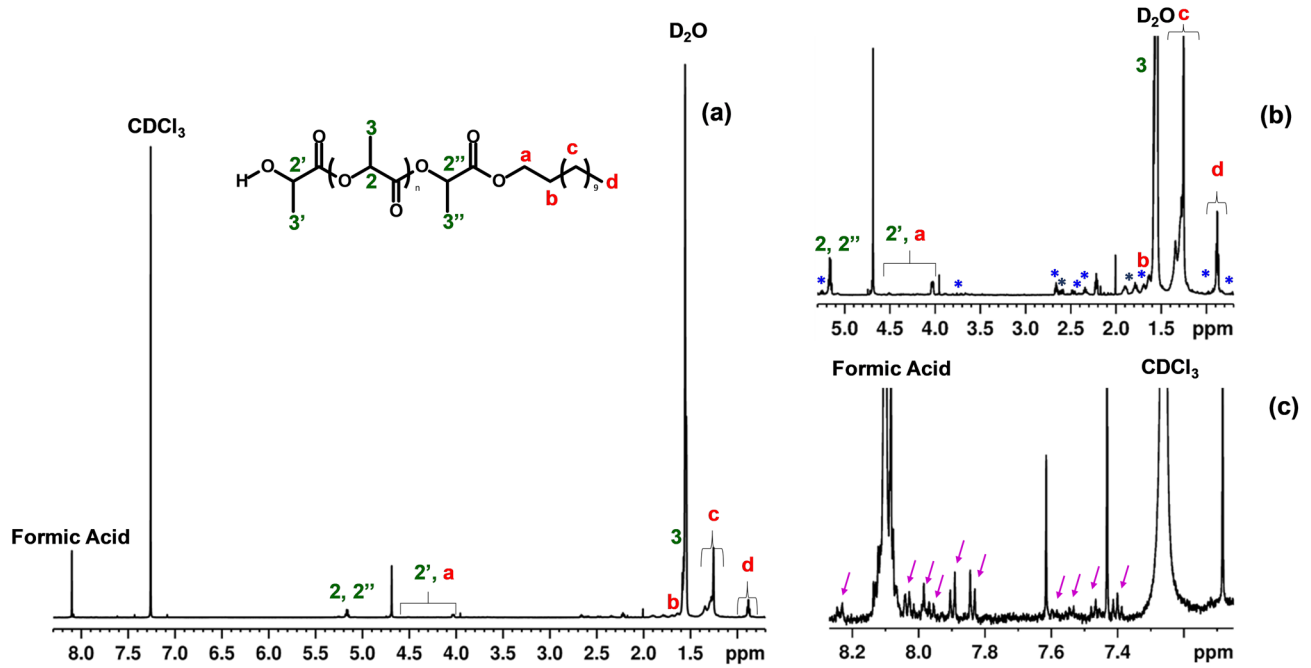

Fig. 6 (a). The ^{1}H NMR spectra of the PLA NPs in $CDCl_3$. Inset: the molecular structure of PLA. The numbers indicate the methyl (–CH_3) and methenyl (═CH–) protons backbone, and the letters correspond to the protons of the lactic acid unit bearing the hydroxyl end group. (b). Zoom-in of the aliphatic region; blue (*) indicates possible signals of PLA of different chain lengths. (c). Zoom-in of the aromatic region; purple arrows indicate some signals of aromatic compounds.

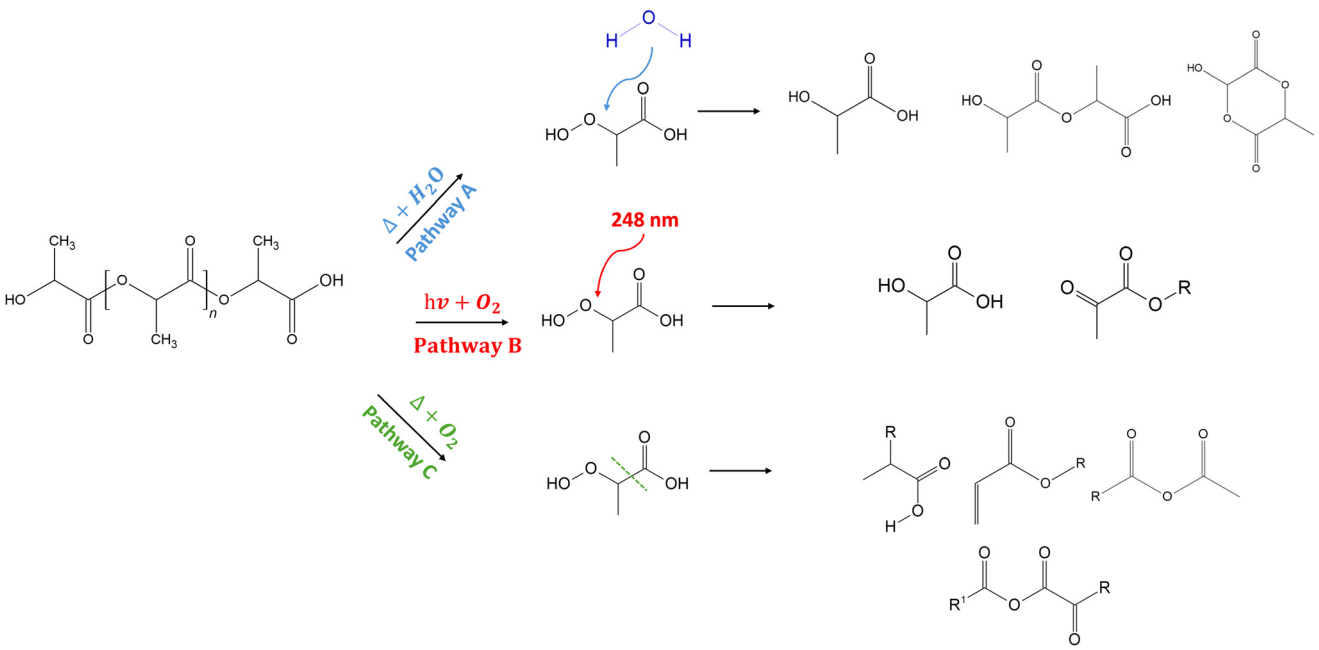

Fig. 7 Common by-products in the hydrolytic (pathway A), photo-oxidative (pathway B), and thermo-oxidative degradation (pathway C) pathways of PLA.[2]

expressed nature of this mechanism. In addition to Norrish type II products, hyperperoxide intermediates can also be formed from the activation of the methine group of the PLA backbone and the insertion of O_2, which can subsequently degrade to carboxylic acids, aldehydes, and diketones.[61] The presence of polar groups on the NP surface observed in Raman and XPS analyses, along with the C═C bonds in the Raman spectrum and the NMR analysis, could indicate the photodegradation pathway of PLA upon interaction with a UV laser.

Finally, PLA can also undergo thermal degradation during laser ablation, predominantly by random chain scissions through non-radical reactions along the polymer backbone, as

shown in the pathway (C). Depending on the point in the backbone at which the reaction occurs, the final product could be a lactide molecule, an oligomeric ring with more than two repeat units, or acetaldehyde plus carbon monoxide.[43,62–64] In addition, the presence of oxygen can also induce thermo-oxidative degradation, inducing chain scission mechanisms, the formation of free radicals, and ester and carbonyl groups.[10] PLA is also reported to form a series of oxidation, fracture, and double bond products after photoaging under low-temperature thermal degradation conditions, including molecular chain fracture, depolymerization, and inter and intramolecular exchange reactions.[65] As observed in the NMR analysis of the NPs, the presence of very weak peaks at the aromatic region may be, indeed, due to the formation of aromatic molecules (like *O*-phthalic acid)[43] as a result of thermo-oxidative degradation, as mentioned above. Overall, from the presented analyses, it may be concluded that the degradation process is a combined mechanism of all three pathways. This leads to the aging of the polymer, causing deterioration of chemical properties[66] by the chain disruption at the ester group and the formation of small-sized compounds and other molecules.[8]

Conclusions

In conclusion, we present an attempt to mimic PLA NPs that would naturally form in aqueous environments due to the environmental degradation of larger plastic fragments. This was succeeded through the fabrication of PLA NPs *via* laser ablation in a water environment, yielding particles characterized by enhanced roundness and heterogeneous size distribution with an average diameter of 54.7 ± 26.7 nm. The NTA analysis also confirms this heterogeneity of the NPs, with 90% of the particles detected falling below 200 nm of hydrodynamic diameter. The analytical techniques adopted corroborated the chemical nature of the developed NPs with some modifications attributed to the primary chain polymer backbone cleavage, with physicochemical attributes corresponding to those of their expected naturally occurring counterparts. Thus, the herein process presents a valuable NPs model for investigating the environmental and biological implications of a biobased polymer like PLA, such as their interactions and potential complex formations with other environmental pollutants and their biotoxicity, persistence, and accumulation mechanisms in biological models, among others. For such large-scale applications, various aspects of the laser ablation process can be optimized for the enhancement of the production yield, such as ablating multiple samples simultaneously through the splitting of the irradiation beam, ensuring continuous exposure to fresh surfaces by moving polymer targets or incorporating continuous flow cells to renew the water medium.

Data availability

The data that support the findings of this study are available from the corresponding author upon reasonable request. In addition, key results relevant to the findings presented in this paper are provided as graphical figures. These figures offer a condensed version of the dataset to facilitate understanding and reproduction of the main results. Researchers interested in obtaining the full dataset or additional details about the methods should contact the corresponding author.

Author contributions

Malavika Manju Sudheer: investigation, methodology, visualization, writing-original draft; Arezou Fazli: methodology, writing-review and editing; Stefania Sganga: investigation, writing-review and editing; Nicola Tirelli: resources; Riccardo Carzino: investigation, writing-review and editing; Marina Veronesi: investigation, writing-review and editing; Kirill Khabarov: investigation; Athanassia Athanassiou: funding acquisition, writing-review and editing; Despina Fragouli: conceptualization, methodology, validation, visualization, writing-review and editing, supervision.

Conflicts of interest

The authors declare no conflicts of interest.

Acknowledgements

This work is part of the "Technologies for Sustainability" Flagship program of the Italian Institute of Technology (IIT). The authors thank Lara Marini and Giacomo Tedeschi from the Smart Materials group for their invaluable technical assistance and input on preparing PLA films. Additionally, the authors acknowledge Doriana Debellis and Federico Catalano from the Electron Microscopy Facility for providing imaging and data analysis support.

References

1 D. Rosato, *Designing with plastics and composites: a handbook*, Springer Science & Business Media, 2013.
2 A. Chamas, H. Moon, J. Zheng, Y. Qiu, T. Tabassum and J. H. Jang, *et al.*, Degradation Rates of Plastics in the Environment, *ACS Sustainable Chem. Eng.*, 2020, **8**(9), 3494–3511.
3 D. K. Barnes, F. Galgani, R. C. Thompson and M. Barlaz, Accumulation and fragmentation of plastic debris in global environments, *Philos. Trans. R. Soc., B*, 2009, **364**(1526), 1985–1998.
4 M. Cole, P. Lindeque, C. Halsband and T. S. Galloway, Microplastics as contaminants in the marine environment: a review, *Mar. Pollut. Bull.*, 2011, **62**(12), 2588–2597.
5 OECD, *Global Plastics Outlook*, 2022.
6 R. Geyer, J. R. Jambeck and K. L. Law, Production, use, and fate of all plastics ever made, *Sci. Adv.*, 2017, **3**(7), e1700782.
7 K. J. Jem and B. Tan, The development and challenges of poly (lactic acid) and poly (glycolic acid), *Adv. Ind. Eng. Polym. Res.*, 2020, **3**(2), 60–70.

8 E. Balla, V. Daniilidis, G. Karlioti, T. Kalamas, M. Stefanidou and N. D. Bikiaris, *et al.*, Poly (lactic Acid): A versatile biobased polymer for the future with multifunctional properties—From monomer synthesis, polymerization techniques and molecular weight increase to PLA applications, *Polymers*, 2021, **13**(11), 1822.
9 Group PMR, *Plastics—The Facts 2018*, Plastics Europe Association of Plastics Manufacturers, 2018.
10 N. M. Ainali, D. Kalaronis, E. Evgenidou, G. Z. Kyzas, D. C. Bobori and M. Kaloyianni, *et al.*, Do poly (lactic acid) microplastics instigate a threat? A perception for their dynamic towards environmental pollution and toxicity, *Sci. Total Environ.*, 2022, **832**, 155014.
11 A. L. Andrady, Microplastics in the marine environment, *Mar. Pollut. Bull.*, 2011, **62**(8), 1596–1605.
12 K. Mattsson, S. Jocic, J. A. de Lima, L.-A. Hansson and A. Gondikas, Nanoplastics in aquatic environments—Sources, sampling techniques, and identification methods, *Microplastic Contamination in Aquatic Environments*, Elsevier, 2024, pp. 381–397.
13 J. Gigault, A. Ter Halle, M. Baudrimont, P.-Y. Pascal, F. Gauffre and T.-L. Phi, *et al.*, Current opinion: what is a nanoplastic?, *Environ. Pollut.*, 2018, **235**, 1030–1034.
14 D. M. Mitrano, P. Wick and B. Nowack, Placing nanoplastics in the context of global plastic pollution, *Nat. Nanotechnol.*, 2021, **16**(5), 491–500.
15 L. Yang, D. Li, Y. Shi, C. Hill, R. Pilliadugula and L. Page, *et al.*, High levels of microparticles release from biodegradable polylactic acid paper cups compared with polyethylene-lined cups, *Chem. Eng. J.*, 2023, **468**, 143620.
16 G. Banaei, A. García-Rodríguez, A. Tavakolpournegari, J. Martín-Pérez, A. Villacorta and R. Marcos, *et al.*, The release of polylactic acid nanoplastics (PLA-NPLs) from commercial teabags. Obtention, characterization, and hazard effects of true-to-life PLA-NPLs, *J. Hazard. Mater.*, 2023, **458**, 131899.
17 H. Tong, X. Zhong, Z. Duan, X. Yi, F. Cheng and W. Xu, *et al.*, Micro-and nanoplastics released from biodegradable and conventional plastics during degradation: formation, aging factors, and toxicity, *Sci. Total Environ.*, 2022, **833**, 155275.
18 M. Tamayo-Belda, C. Venâncio, F. Fernandez-Piñas, R. Rosal, I. Lopes and M. Oliveira, Effects of petroleum-based and biopolymer-based nanoplastics on aquatic organisms: a case study with mechanically degraded pristine polymers, *Sci. Total Environ.*, 2023, **883**, 163447.
19 X.-F. Wei, A. J. Capezza, Y. Cui, L. Li, A. Hakonen and B. Liu, *et al.*, Millions of microplastics released from a biodegradable polymer during biodegradation/enzymatic hydrolysis, *Water Res.*, 2022, **211**, 118068.
20 B. Koelmans, S. Pahl, T. Backhaus, F. Bessa, G. van Calster and N. Contzen, *et al.*, *A scientific perspective on microplastics in nature and society*, SAPEA, 2019.
21 P. Kershaw, A. Turra and F. Galgani, *Guidelines for the monitoring and assessment of plastic litter and microplastics in the ocean*, 2019.
22 R. C. Hale, Analytical challenges associated with the determination of microplastics in the environment, *Anal. Methods*, 2017, **9**(9), 1326–1327.
23 C. Zarfl, Promising techniques and open challenges for microplastic identification and quantification in environmental matrices, *Anal. Bioanal. Chem.*, 2019, **411**, 3743–3756.
24 E. D. Okoffo and K. V. Thomas, Quantitative analysis of nanoplastics in environmental and potable waters by pyrolysis-gas chromatography–mass spectrometry, *J. Hazard. Mater.*, 2024, **464**, 133013.
25 N. P. Ivleva, Chemical analysis of microplastics and nanoplastics: challenges, advanced methods, and perspectives, *Chem. Rev.*, 2021, **121**(19), 11886–11936.
26 E. Kelpsiene, M. Rydberg, M. T. Ekvall, M. Lundqvist and T. Cedervall, Prolonged survival time of Daphnia magna exposed to polylactic acid breakdown nanoplastics, *PLoS One*, 2023, **18**(9), e0290748.
27 G. An, J. Na, J. Song and J. Jung, Chronic toxicity of biodegradable microplastic (Polylactic acid) to Daphnia magna: A comparison with polyethylene terephthalate, *Aquat. Toxicol.*, 2024, **266**, 106790.
28 M. Alaraby, D. Abass, M. Farre, A. Hernández and R. Marcos, Are bioplastics safe? Hazardous effects of polylactic acid (PLA) nanoplastics in Drosophila, *Sci. Total Environ.*, 2024, 170592.
29 J. Domenech, A. Villacorta, J. F. Ferrer, R. Llorens, R. Marcos and A. Hernández, *et al.*, In vitro cell-transforming potential of secondary polyethylene terephthalate and polylactic acid nanoplastics, *J. Hazard. Mater.*, 2024, 134030.
30 L. A. Parker, E. M. Höppener, E. F. van Amelrooij, S. Henke, I. M. Kooter and K. Grigoriadi, *et al.*, Protocol for the production of micro- and nanoplastic test materials, *Microplast. Nanoplast.*, 2023, **3**(1), 10.
31 J. Caldwell, R. Lehner, S. Balog, C. Rhême, X. Gao and D. Septiadi, *et al.*, Fluorescent plastic nanoparticles to track their interaction and fate in physiological environments, *Environ. Sci.: Nano*, 2021, **8**(2), 502–513.
32 D. Magrì, P. Sánchez-Moreno, G. Caputo, F. Gatto, M. Veronesi and G. Bardi, *et al.*, Laser ablation as a versatile tool to mimic polyethylene terephthalate nanoplastic pollutants: characterization and toxicology assessment, *ACS Nano*, 2018, **12**(8), 7690–7700.
33 V. Tolardo, D. Magrì, F. Fumagalli, D. Cassano, A. Athanassiou and D. Fragouli, *et al.*, In Vitro High-Throughput Toxicological Assessment of Nanoplastics, *Nanomaterials*, 2022, **12**(12), 1947.
34 V. Tolardo, A. Romaldini, F. Fumagalli, A. Armirotti, M. Veronesi and D. Magrì, *et al.*, Polycarbonate nanoplastics and the in vitro assessment of their toxicological impact on liver functionality, *Environ. Sci.: Nano*, 2023, **10**(5), 1413–1427.
35 I. Elaboudi, S. Lazare, C. Belin, D. Talaga and C. Labrugère, From polymer films to organic nanoparticles suspensions by means of excimer laser ablation in water, *Appl. Phys. A: Mater. Sci. Process.*, 2008, **93**, 827–831.

36 A. Kanitz, M. Kalus, E. Gurevich, A. Ostendorf, S. Barcikowski and D. Amans, Review on experimental and theoretical investigations of the early stage, femtoseconds to microseconds processes during laser ablation in liquid-phase for the synthesis of colloidal nanoparticles, *Plasma Sources Sci. Technol.*, 2019, **28**(10), 103001.
37 T. Lippert, UV laser ablation of polymers: from structuring to thin film deposition, *Laser-Surface Interactions for New Materials Production: Tailoring Structure and Properties*, Springer, 2009, pp. 141–175.
38 L. M. F. Batista, M. Moody, C. Weththasingha, E. Kaplan, I. Faruque and M. S. El-Shall, *et al.*, Understanding photochemical pathways of laser-induced metal ion reduction through byproduct analysis, *Phys. Chem. Chem. Phys.*, 2023, **25**(28), 18844–18853.
39 J. S. Böke, J. Popp and C. Krafft, Optical photothermal infrared spectroscopy with simultaneously acquired Raman spectroscopy for two-dimensional microplastic identification, *Sci. Rep.*, 2022, **12**(1), 18785.
40 J.-H. Wu, M.-S. Yen, C.-P. Wu, C.-H. Li and M. Kuo, Effect of biaxial stretching on thermal properties, shrinkage and mechanical properties of poly (lactic acid) films, *J. Polym. Environ.*, 2013, **21**, 303–311.
41 G. Tamburini, S. Bertagnoli, G. Tarricone, S. Piva, A. Sassella and R. Lorenzi, *et al.*, Early stages of X-ray induced molecular unit modifications in poly (lactic acid), *Polym. Degrad. Stab.*, 2023, **216**, 110485.
42 P. Larkin, in *Infrared and Raman Spectroscopy*, ed. P. Larkin, Elsevier, Oxford, 2011, ch. 6 - IR and Raman Spectra-Structure Correlations: Characteristic Group Frequencies, pp. 73–115.
43 S. Teixeira, K. M. Eblagon, F. Miranda, M. F. R. Pereira and J. L. Figueiredo, Towards controlled degradation of poly (lactic) acid in technical applications, *C*, 2021, **7**(2), 42.
44 X. Wu, H. Zhang, J. Chen, F. Tan, R. Cai and Y. Wang, Photoaging Promotes Toxic Micro/Nanoplastics Release from PLA/PBAT Biodegradable Plastic in Gastrointestinal Condition, *Environ. Health*, 2025, DOI: **10.1021/envhealth.4c00209**, Article ASAP.
45 J. Gigault, H. El Hadri, B. Nguyen, B. Grassl, L. Rowenczyk and N. Tufenkji, *et al.*, Nanoplastics are neither microplastics nor engineered nanoparticles, *Nat. Nanotechnol.*, 2021, **16**(5), 501–507.
46 J. Zhang, X. Xia, W. Huang, Y. Li, X. Lin and Y. Li, *et al.*, Photoaging of biodegradable nanoplastics regulates their toxicity to aquatic insects (Chironomus kiinensis) by impairing gut and disrupting intestinal microbiota, *Environ. Int.*, 2024, 108483.
47 J. Fei, H. Xie, Y. Zhao, X. Zhou, H. Sun and N. Wang, *et al.*, Transport of degradable/nondegradable and aged microplastics in porous media: Effects of physicochemical factors, *Sci. Total Environ.*, 2022, **851**, 158099.
48 E. Sambha'a, A. Lallam and A. Jada, Effect of hydrothermal polylactic acid degradation on polymer molecular weight and surface properties, *J. Polym. Environ.*, 2010, **18**(4), 532–538.
49 A. J. Antończak, B. D. Stępak, K. Szustakiewicz, M. R. Wójcik and K. M. Abramski, Degradation of poly (l-lactide) under CO2 laser treatment above the ablation threshold, *Polym. Degrad. Stab.*, 2014, **109**, 97–105.
50 P. Rytlewski, W. Mróz, M. Żenkiewicz, J. Czwartos and B. Budner, Laser induced surface modification of polylactide, *J. Mater. Process. Technol.*, 2012, **212**(8), 1700–1704.
51 Degradation of poly (L-lactide) under femtosecond laser treatment, *Laser-based Micro-and Nanoprocessing XII*, ed. A. J. Antończak, B. D. Stępak, M. Gazińska and K. Szustakiewicz, SPIE, 2018.
52 P. Bhati, A. Srivastava, R. Ahuja, P. Chauhan, P. Vashisth and N. Bhatnagar, Physicochemical properties of UV-irradiated, biaxially oriented PLA tubular scaffolds, *Polymers*, 2023, **15**(5), 1097.
53 H. Jiang, Y. Wang, J. Sun, Y. Mao, S. Que and Y. Lin, *et al.*, The aging behavior of degradable plastic polylactic acid under the interaction of environmental factors, *Environ. Geochem. Health*, 2024, **46**(5), 163.
54 J. M. Pérez, C. Ruiz and I. Fernández, Synthesis of a Biodegradable PLA: NMR Signal Deconvolution and End-Group Analysis, *J. Chem. Educ.*, 2021, **99**(2), 1000–1007.
55 P. Rizzarelli, G. Piredda, S. La Carta, E. F. Mirabella, G. Valenti and R. Bernet, *et al.*, Characterization and laser-induced degradation of a medical grade polylactide, *Polym. Degrad. Stab.*, 2019, **169**, 108991.
56 S. Therias, J.-F. Larché, P.-O. Bussiere, J.-L. Gardette, M. Murariu and P. Dubois, Photochemical behavior of polylactide/ZnO nanocomposite films, *Biomacromolecules*, 2012, **13**(10), 3283–3291.
57 S. Lomakin, Y. Mikheev, S. Usachev, S. Rogovina, L. Zhorina and E. Perepelitsina, *et al.*, Evaluation and Modeling of Polylactide Photodegradation under Ultraviolet Irradiation: Bio-Based Polyester Photolysis Mechanism, *Polymers*, 2024, **16**(7), 985.
58 S. De Jong, E. R. Arias, D. Rijkers, C. Van Nostrum, J. Kettenes-Van den Bosch and W. Hennink, New insights into the hydrolytic degradation of poly (lactic acid): participation of the alcohol terminus, *Polymer*, 2001, **42**(7), 2795–2802.
59 N. Kondo and M. Terakawa, Biodegradability of poly(lactic-co-glycolic acid) irradiated with femtosecond laser pulses without material removal, *Appl. Phys. A: Mater. Sci. Process.*, 2019, **125**, 135.
60 E. Castro-Aguirre, F. Iniguez-Franco, H. Samsudin, X. Fang and R. Auras, Poly (lactic acid)—Mass production, processing, industrial applications, and end of life, *Adv. Drug Delivery Rev.*, 2016, **107**, 333–366.
61 A. V. Janorkar, A. T. Metters and D. E. Hirt, Degradation of poly (L-lactide) films under ultraviolet-induced photografting and sterilization conditions, *J. Appl. Polym. Sci.*, 2007, **106**(2), 1042–1047.
62 I. McNeill and H. Leiper, Degradation studies of some polyesters and polycarbonates—2. Polylactide: degradation under isothermal conditions, thermal degradation mechanism and photolysis of the polymer, *Polym. Degrad. Stab.*, 1985, **11**(4), 309–326.
63 H. Zou, C. Yi, L. Wang, H. Liu and W. Xu, Thermal degradation of poly (lactic acid) measured by

thermogravimetry coupled to Fourier transform infrared spectroscopy, *J. Therm. Anal. Calorim.*, 2009, **97**, 929–935.

64 F.-D. Kopinke, M. Remmler, K. Mackenzie, M. Möder and O. Wachsen, Thermal decomposition of biodegradable polyesters—II, Poly (lactic acid), *Polym. Degrad. Stab.*, 1996, **53**(3), 329–342.

65 X. Wang, J. Chen, W. Jia, K. Huang and Y. Ma, Comparing the Aging Processes of PLA and PE: The Impact of UV Irradiation and Water, *Processes*, 2024, **12**(4), 635.

66 N. F. Zaaba and M. Jaafar, A review on degradation mechanisms of polylactic acid: Hydrolytic, photodegradative, microbial, and enzymatic degradation, *Polym. Eng. Sci.*, 2020, **60**(9), 2061–2075.